Turning without fins: Quantifying the distinct kinematics and vortex dynamics of maneuvering swimming snakes

Elizabeth Gregorio *
PMMH, UMR 7636 CNRS, ESPCI Paris–Université PSL, Sorbonne Université, Université Paris Cité, Paris, France and MECADEV, UMR 7179, Département Adaptation du Vivant, MNHN/CNRS, Paris, France

Ramiro Godoy-Diana
PMMH, UMR 7636 CNRS, ESPCI Paris–Université PSL, Sorbonne Université, Université Paris Cité, Paris, France

Anthony Herrel
MECADEV, UMR 7179, Département Adaptation du Vivant, MNHN/CNRS, Paris, France; Department of Biology, Evolutionary Morphology of Vertebrates, Ghent University, Ghent, Belgium; Functional Morphology Laboratory, Department of Biology, University of Antwerp, Antwerp, Belgium; and Naturhistorisches Museum Bern, Bern, Switzerland

(Received 20 October 2025; accepted 23 July 2026; published 31 August 2026)

The agile turning maneuvers of anguilliform swimmers remain one of the least studied aspects of aquatic locomotion, despite being crucial for survival in underwater environments. To change direction, animals must find a balance between minimizing their moment of inertia and maximizing torque. Anguilliform swimmers, like snakes, are highly maneuverable and accomplish this goal without the aid of limbs or pectoral fins. In this study, we quantify the differences between turning and forward swimming kinematics and hydrodynamics. We present flow field and body deformation measurements taken simultaneously by combining a volumetric three-component defocusing digital particle-tracking velocimetry system with a camera mounted above the tank for swimming kinematics. We determine how snakes manipulate their body position to change swimming direction by analyzing the swimming kinematics of six turns by six individuals as 2D projections (five *Natrix maura* and one *Nerodia rhombifer*). Analyses of the body kinematics show that snakes curl their body inwards to shift their center of mass and reduce their moment of inertia to perform faster turns. The volumetric wake measurements allow us to quantify the timing between the turning kinematics and vortex shedding and to compare it with forward swimming measurements. Our results indicate that snakes can generate substantially stronger vortices when turning; for example, the vortex force can be as much as 2.5–8.6× larger when compared to forward swimming. We also use volumetric wake measurements to show that the vortices shed during a turn have the same tubular vortex pair composition as forward swimming. These results help explain how elongated anguilliform swimmers change swimming direction. They widen our understanding of how animals use transient maneuvers to navigate aquatic environments, with implications for both natural swimmers and underwater robots.

DOI: 10.1103/c57h-kx57

I. INTRODUCTION

Anguilliform swimmers, like snakes, use their entire body to generate propulsion [1]. They generate and build vorticity along their body length with full body undulations and surface rotation. This vorticity is shed as large vortex structures near the posterior part of their body with active tail sweeping [2,3]. Three-dimensional wake measurements of forward swimming in snakes reveal that this posterior vortex structure has a hairpin-like shape [4], which matches results from computational studies [5,6].

Aquatic animals explore their environments with a combination of swimming behaviors such as cruising, accelerating, and maneuvering [7]. Of these cruising—forward swimming at a constant speed—is the most commonly studied. Snakes and other anguilliform swimmers have a highly maneuverable flexible elongated body. It enables a variety of movements such as swimming backwards, navigating narrow crevices, and coiling tightly or knotting to stabilize in the water column. [1,8–10]. In fact, snakes have 11 documented locomotor modes facilitating their navigation and maneuverability in a variety of environments [11]. Yet little is known about how these animals change swimming directions.

Fast starts may be the best studied transient swimming maneuvers. These are performed by some fish to accelerate and change direction during predator-prey interactions by curving their body into a S or C shape in preparation for a propulsive stroke [12]. Simulations of the C-start behavior show the fish uses this pronounced body bend to trap and accelerate a large amount of fluid for propulsion [13]. The resulting jet has a greater average nondimensional circulation than the typical

*Contact author: elizabeth.gregorio@espci.fr

forward swimming wake [14]. In some cases, the fish interact with their wake during the start and following swimming cycles [15]. These are just a few examples highlighting how the kinematics and resulting wake for fast start behaviors differ from forward swimming.

Not all turns include large changes in speed, as is characteristic to the fast start behavior. In fact, the speed of the turn has been shown to have a significant effect on kinematics and angular velocity in a study using bluegill sunfish [16]. Some examples of recent studies performing wake measurements of turning maneuvers performed by aquatic animals without changes in speed include jellyfish (*Aurelia aurita*) [17,18], squid (*Lolliguncula brevis*) [19], zebrafish (*Danio rerio*) [17,20], and giant danio (*Devario aequipinnatus*) [21]. These studies highlight a complex mechanical problem that animals are confronted with when turning to maximize torque or minimize moment of inertia [17]. Both quantities are dependent on the characteristic radius, so finding a balance is not insignificant. Zebra fish and jellyfish accomplish this by exploiting their flexibility to manipulate the location of their propulsive surface (caudal fins and bell margin) to initiate the turn [17,18,20]. However, this result cannot be easily extended to snakes and other anguilliform swimmers who use their whole body as a propulsive surface.

Much of the existing literature on how snakes might achieve maneuverability comes from bio-inspired robotics. Snakes' adaptability to different environments makes them an attractive model system, and many snake-like robots have been developed over the years. Snake-like robots typically use a symmetric traveling wave to produce forward movement. In this case, turning is achieved through amplitude and phase modulation of the traveling wave [22]. While this method is effective, applying bio-inspired methods reduces the minimum turning radius. Examples of this include head steering [23] and the omega gait [24,25]. Bio-inspired swimming gaits, like applying a traveling wave with increasing amplitude, also achieve higher performance [26]. This indicates that there is potential to improve swimming and maneuvering in snake-like robotics by investigating how these animals achieve turning in nature. The results presented in this study provide a window into how snakes perform maneuvers and provide needed examples for bio-inspired robotics.

The goal of this study is to quantify how snake turning maneuvers are different from forward swimming. Their mode of swimming and finless elongated body differentiates them from species whose turning mechanics have been previously studied, and these characteristics likely require a different turning mechanism. Here we begin to address this question by quantifying the kinematics of forward-swimming and turning snakes to understand how they differ. We combine this analysis with a comparison of wake measurements taken while a snake is performing a turn with forward swimming sequences.

II. MATERIALS AND METHODS

Our experiment captures the swimming kinematics and volumetric wake measurements of swimming snakes with a dual system (Fig. 1). We fill the plexiglass water tank ($210 \times 18 \times 30$ cm) to a height of 22 cm and seed it with 50 μm polyamide particles (PSP-50, Dantec Dynamics) to a concentration of roughly 5×10^{-2} ppp [Fig. 1(a)]. A 200 mJ dual head Nd:YAG laser (Quantel Evergreen) mounted above the tank illuminates the particles with a cone of light created by expanding the beam with two −25 mm cylindrical lenses [Fig. 1(b)]. We capture particle movement with volumetric three-component defocusing digital particle tracking velocimetry (DDPTV; V3V-9000-CS system, TSI) using a three-camera array (Powerview Plus 4MP-HS) mounted on an equilateral triangular frame (170 mm side length, V3V 9000-CS) and 50 mm camera lenses (Nikon AF Nikkor, aperture $f/16$). The measurement volume is centered in the z and y axes of the tank at the intersection of the camera array's field of view and the laser cone [$18 \times 12 \times 18$ cm, Fig. 1(d)]. Another camera captures the swimming kinematics in dorsal view from above the tank [Fig. 1(e)]. The dual system is synchronized to record the snake's movements at 14 Hz.

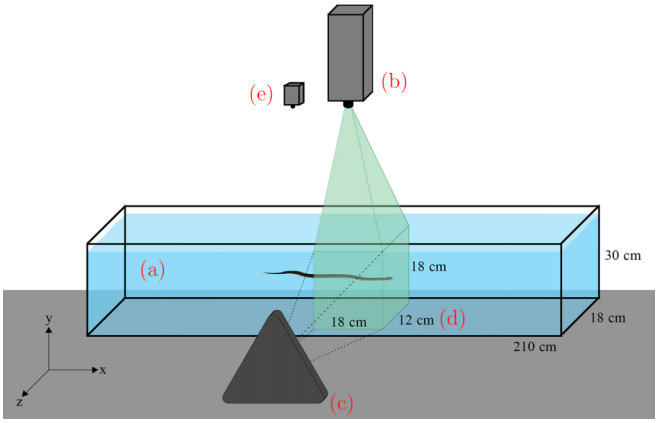

FIG. 1. Experimental setup for measuring the 3D wake of swimming snakes using a V3V system: (a) water tank (b) Nd:YAG laser, (c) camera array, (d) measurement volume ($18 \times 12 \times 18$ cm), (e) kinematics camera.

In each experiment, we place a live snake in the tank and encourage it to swim, completely submerged within the bulk of the water. The snakes voluntarily perform either forward swimming or turning behaviors in each of the recordings. These recordings consist of 44 swimming sequences with five *Natrix maura* individuals and 10 with one *Nerodia rhombifer* individual over 16 nonconsecutive days. These snakes are chosen due to their comparable size and ability to fully maneuver within the water tank sufficiently far from the walls. We include all results where there are coherent vortices and the surface of the water remains still. We explain these choices in more detail later in this section.

Deriving the volumetric wake measurements requires several postprocessing steps. We mask the body of the snake in each image using threshold functions in the MATLAB Image Processing Toolbox. The INSIGHT V3V-4G software processes these images into a velocity field on a randomly spaced grid within the measurement volume. We then use a Gaussian-weighted algorithm [27] to interpolate these velocity vectors onto an evenly spaced vector grid ($74 \times 74 \times 43$) with 2.5 mm resolution (45 vectors per body length for individual no. 1). Stin *et al.* [4] explains the main steps of data processing with this software.

We import the resulting velocity fields into MATLAB with a custom code for visualization and computation. We calculate the Q criterion of the vector field to identify vortices as regions where the vorticity is greater than the strain rate. We choose the value of Q criterion to apply to each swimming sequence by determining the minimum value that reveals the coherent vortex structures while excluding small structures arising from noise. This noise is typically a result of water movement from handling the snake. We plot the surfaces of the coherent vortex structures and use their vorticity fields for our computations. After performing these steps with all the recorded sequences, there are coherent vortices with minimal to no noise in a total of three sequences for the *Nerodia rhombifer* and five for the *Natrix maura*, one of which includes a turn. Of those sequences, we include all in which the surface of the water remains still, allowing us to perform the kinematic analysis.

Previous studies directly calculate the forces applied during the turn by deriving the pressure fields close to the body of the turning animal with 2D PIV methods [17,20]. However, the temporal and spatial resolution we achieve with volumetric DDPTV to capture the fluid movement produced by free-swimming snakes requires a different approach.

We apply Saffman's [28] definition of hydrodynamic impulse to quantify the momentum change required to instantaneously generate the coherent vortices from a fluid at rest:

$$J = \frac{\rho}{2}\int_V \vec{x} \times \vec{\omega} dV, \tag{1}$$

where ρ is fluid density, V is vortex volume, x is the vector pointing from measurement volume's center to the center of V, and ω is the vorticity field. The J is calculated for the entire measurement volume throughout the swimming sequence.

When a vortex is shed, there is a sudden change in J, which eventually returns to zero as the vortex dissipates. We use a quadratic polynomial to find the line of best fit through these points, chosen to capture the curvature. We calculate the vortex force vector ($F_{(x,y,z)} = dJ_{(x,y,z)}/dt$) by taking the time derivative of the line of best fit and interpreting the slope as the vortex force component, and the vortex force magnitude according to convention ($F_v = \sqrt{F_x^2 + F_y^2 + F_z^2}$). We use this to determine the force coefficient:

$$C_F = \frac{F_v}{0.5\rho S U^2}, \tag{2}$$

where S is the snake's cross-sectional area calculated with the diameter at the largest section of the snake and U is the characteristic velocity for the center of mass (U_{com}) or tail (U_{tail}).

To quantify the swimming kinematics, we identify the snake's body and digitize it as a binary mask in the frames captured by the kinematics camera. We use this 2D projection to compute the moment of inertia, the distance and angle between the head and the tail, and the displacement of the head, tail, and center of mass. This captures the overall dynamics of the snake's movement, excluding any out-of-plane movements, which introduces some uncertainty. Nevertheless, our analysis and results are practical for applications in bio-inspired robotics as demonstrated in [24,25,29].

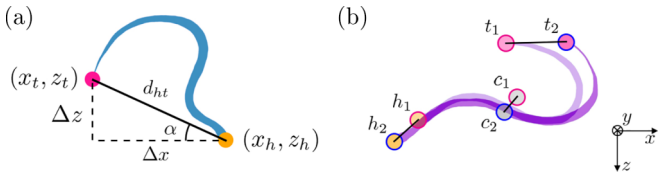

FIG. 2. Demonstration of values used in Eqs. (4) and (5).

To estimate the moment of inertia (I), we first approximate the snake's center of mass using the SCIPY [30] `center_of_mass()` function. With this choice we assume that the snake is swimming in the x-z plane and that the mass is evenly distributed. We use a thinning function to find the snakes centerline, divide the body into N segments, and apply

$$I = \sum_{i=1}^{N} a_i r_i^2, \tag{3}$$

where a_i is the area of each segment along the centerline and r_i is the distance between the centroid of the segment and the snake's center of mass. This method of estimating the moment of inertia follows the standard established in Dabiri *et al.* [17].

We calculate the distance between the snake's head and tail (d), as a proxy for quantifying the deformation of the snake's body:

$$d = \frac{d_{ht}}{d_{bl}} = \frac{\sqrt{(x_h - x_t)^2 + (z_h - z_t)^2}}{d_{bl}}, \tag{4}$$

where the first point of the centerline is the head (x_h, z_h) and the last point is the tail (x_t, z_t). We normalize this quantity by dividing by the snake's body length (d_{bl}). Next, we calculate the angle (α) of the snake's body position:

$$\alpha = \arctan 2(\Delta z, \Delta x) \times \frac{180}{\pi}, \tag{5}$$

where Δx and Δz are the distance between the head and tail in the x and z direction, respectively. We normalize the results so that α begins at 0° regardless of the initial swimming direction of the snake by shifting them accordingly. Finally, we calculate the displacement of the snake's head (h), tail (t), and center of mass (c) between each time step. Figures 2(a) and 2(b) demonstrate the location of the points in Eqs. (4) and (5) on a turning snake.

In this study, we present results for six voluntary turns performed by six individuals in a roughly 2D plane away from the walls of the water tank. We refer to them by their turn number as established in Figs. 3 and 4 where nos. 1 and 3–6 are *Natrix maura* and no. 2 is *Nerodia rhombifer*. We compare these results to forward swimming sequences for the same individuals. We include DDPTV results for the sequences where the snake swam within the measurement volume. These results include the first turn (*Natrix maura*: 6.1 g, 113 mm) and forward swimming sequences for the individuals that performed turns no. 2 and no. 6. Turns no. 2–6 were performed within the field of view for the kinematics camera, and their measurement details can be found in Fig. 8 in the Appendix. The individuals that performed turns no. 2 and 6 completed one and two forward swimming cycles, respectively, within the measurement volume during different recording sessions than their turn. We use the wake measurements for insight into

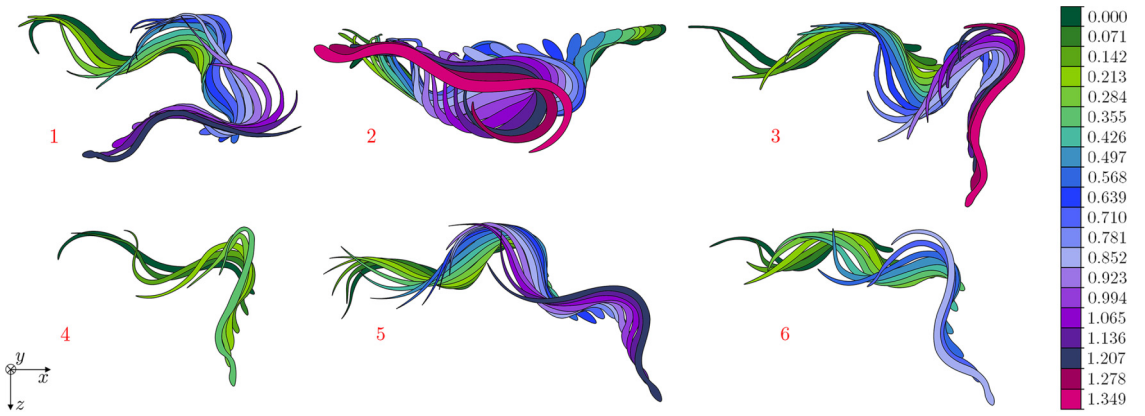

FIG. 3. Superimposed swimming kinematics for turns no. 1–6 with 0.071 s between each body position, as demonstrated by the color bar (turns no. 1 and 3–6 *Natrix maura*; turn no. 2 *Nerodia rhombifer*).

the 3D nature of the snake's turn, to investigate the timing between the swimming kinematics and vortex shedding, and to compare vortex shedding events generated during turning and forward swimming.

III. RESULTS AND DISCUSSION

Six snakes performed voluntary turns following distinct swimming trajectories. In Fig. 3 we superimpose all of the kinematics taken from the dorsal view (x-z plane). This representation highlights the different types of turns and the turning radius. The body positions and center of mass at each time step for turn no. 1 are included in Fig. 6(a) and for turns no. 2–6 in Fig. 8 in the Appendix.

Turns no. 5 and 6 follow a gentle curve, which looks similar to the head steering maneuver performed by a snake-like robot in Shi *et al.* [23], and in turn no. 2 the snake performs a 180° turn similar to the omega gait in Wang *et al.* [24]. However, closer inspection of the no. 2 kinematics shows that it folds its body like an accordion to bring its head and tail closer together instead of directly bringing its head and tail together. The other three turns (no. 1, 3, and 4) perform turning maneuvers that diverge from what has been reported in bio-inspired robotics and can serve as additional sources of inspiration for snake-like robots.

In Fig. 4 we present the quantitative kinematic analysis results. In each case we compare the results measured during the turn to a forward swimming sequence for the same individual. The forward swimming results are represented as the average (dashed line) and the standard deviation (shaded region) of the values in Fig. 9 in the Appendix.

Figure 4(a) shows that d and I/I_{SS} have similar trends, which indicates that the snake is decreasing its moment of inertia by drawing its head and tail closer together. We see a clear distinction in I/I_{ss} and d between the snakes that swam along a curve and those who followed other trajectories. The I/I_{ss} and d for turns no. 5 and 6 stay within or above the typical forward swimming range, while the other snakes significantly decrease their I/I_{ss} while turning. In fact, the lowest values of moment of inertia for turns no. 1–4 is 1.6–3× less than the average value during forward swimming. While these turns follow a wide variety of kinematics, they share a common moment of inertia profile. This shows that snakes decrease their moment of inertia when they perform a turn over a shorter time period.

The variety of turning maneuvers is reflected in the progression of body angle (α) in Fig. 4(b). We see that for turns no. 1 and 2 the snake rotates 180° to swim in the opposite direction. In turn no. 2 the snake does so by rapidly increasing its α from 11° to 127° in one frame (0.071 s), whereas, in turn no. 1 the snake completes a U-shaped turn by continually increasing its α with two local minima in I/I_{ss}, indicating this turn is composed of two roughly 90° turns. In turns no. 5 and 6 the snake swims along a curve steadily increasing its α to reach different maximum angle measurements: 70° and 55°, respectively. This result is indeed comparable to head steering [23]. Each of the other turns (no. 1–4) are completed over a shorter time and a smaller turning radius, as seen in Fig. 3. In fact, in turn no. 4 the snake reaches a similar turn angle as no. 5, three times faster. The superimposed kinematics for turns no. 3 and 4 suggest a 90° turn, as their initial and final body positions appear to be perpendicular. However, their final α is 105° and 73° respectively, which demonstrates the versatility of this type of turn.

The volumetric wake measurements for turn no. 1 allows us to better understand its turning maneuver. The 3D wake measurements of this turn are shown in Fig. 5 with the corresponding kinematics highlighted by a red box in Fig. 6(a). Before the first frame, the snake pulls its body into a C-shape. Its tail flicks in the positive z direction, generating a vortex that is visible in the first five frames of Fig. 5 (1–1.29 s). Then the snake turns its head in the negative x direction, generating a vortex that is visible in frames 3–8 (1.14–1.5 s). In frame 9 (1.57 s), the body of the snake is curved like a hook and then the snake uncurls to complete the turn, generating a large vortex that is visible for the rest of the time series (1.57–1.79 s). The first frame where each of these vortex shedding events is visible is highlighted in Fig. 5 with a dashed red box.

When engaged in forward swimming, snakes and other anguilliform swimmers typically shed a vortex at each bend along the body [4]. It is interesting that when turning we see vortex shedding events after large movements of the snake instead of at every curve along the snake's body. These nonvortex shedding movements are undoubtedly building up vorticity along the body, as has been measured in forward swimming of lamprey and eels [2,3] that our measurements do

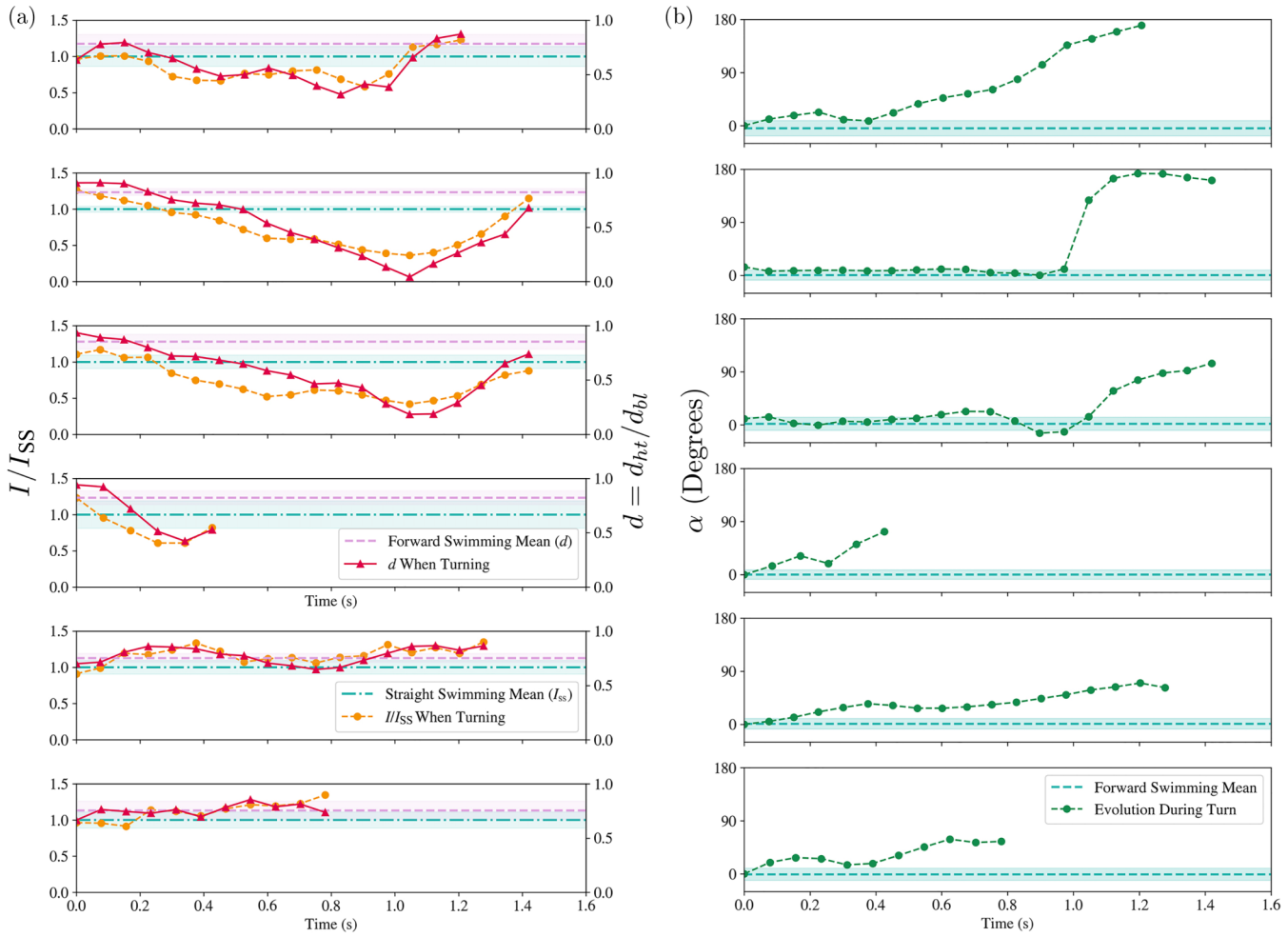

FIG. 4. Quantification of turning kinematics in order of decreasing final angle: (a) moment of inertia [I/I_{ss}, Eq. (3)] and distance between the head and tail [d, Eq. (4)], (b) angle between the head and tail [α, Eq. (5)]. Forward swimming values are represented as the average and standard deviation (see Fig. 8 in the Appendix) (turns no. 1 and 3–6 *Natrix maura*, no. 2 *Nerodia rhombifer*).

not capture. Our methodology allows us to resolve the larger coherent vortices after they are shed. Still, our results suggest that turning snakes rely on body rearrangement movements that do not necessarily shed large vortices.

By quantifying the wake, we can investigate the turning mechanism through the timing of vortex shedding and momentum transfer to the fluid. We calculate the hydrodynamic impulse (J_x, J_y, and J_z) for the entire volume at each time step and report it for the full 4 s recording. The J is calculated in the Eulerian reference frame with the positive x axis aligned to the original swimming direction of the snake. This is demonstrated in the kinematics [Fig. 6(a)] where the snake swims along the positive x axis from 0 to 1 s and then along the negative x axis after completing its turn (1.79 s). The impulse plot does not show any deviation from 0 N/s until the turn begins because this portion of forward swimming is outside the measurement volume. The spike after the turning section around the 2 s mark is due to the second portion of forward swimming. The wake measurements for this portion of forward swimming reveals two tubular vortices with opposite directions, similar to the results presented by Stin *et al.* [4]. The kinematics of this portion are typical for forward swimming and are used as the reference average and standard deviation in Fig. 4, with the true values in Fig. 9 in the Appendix. However, the turning vortices have not yet dissipated, so we do not present this vortex event for hydrodynamic analysis. After this, the snake swims out of the field of view and the measured hydrodynamic impulse returns to 0 N/s.

The turning portion of the hydrodynamic impulse measurement is highlighted in red [Fig. 6(c)]. Each of the three major vortex events is identifiable on this impulse plot by a gray dotted line. The first two vortex events overlap, which likely decreases the calculated J (we will return to this later in the discussion). The third vortex has the largest J peaks and thus represents the largest transfer of momentum from the snake to the fluid. In fact, at 1.57 s when the vortex is at its largest size, 47% of the impulse is in the x direction, 46% in the y direction, and 5% in the z direction. After this peak, the vortex's impulse dissipates in size in the x and y directions, while in the z direction the impulse increases before dissipating.

Figure 6(d) shows the kinematics quantification with gray lines to indicate the first frame for each vortex observation. The first and third vortices appear directly after the minimum values in the snake's moment of inertia and after a large tail displacement (d_m) indicating they are generated by tail

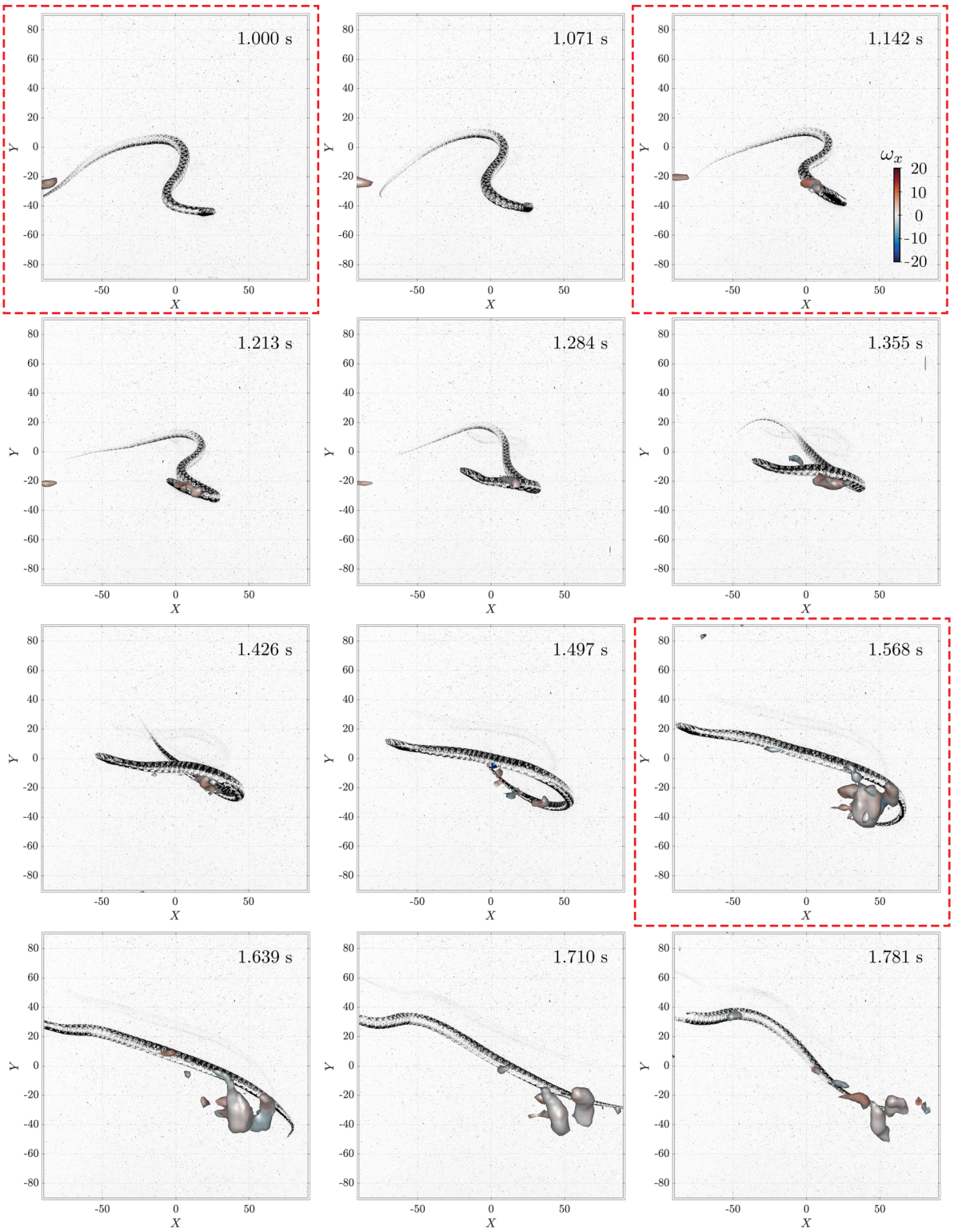

FIG. 5. Time series of wake measurements taken for turn no. 1 (*Natrix maura*). The time separation between images is of 0.071 s. The positive x axis is aligned with the snakes original swimming direction.

movement. The α progresses steadily from 0° to 180°, a rise that starts just after the first vortex event. The third vortex event appears immediately after the α increases by the largest margin in the recording (33°, $t = 1.50 - 1.57$). This timing suggests that the snake sheds vortices after reaching a low moment of inertia to enable turning.

Anguilliform swimmers typically shed hairpin-shaped vortices that are composed of a tubular vortex pair, with each vortex having an opposite vorticity direction. This shape has been demonstrated both computationally [5,6] and experimentally for swimming snakes [4]. In Fig. 7 we see snapshots of all analyzed vortex events, with a second panel that shows the

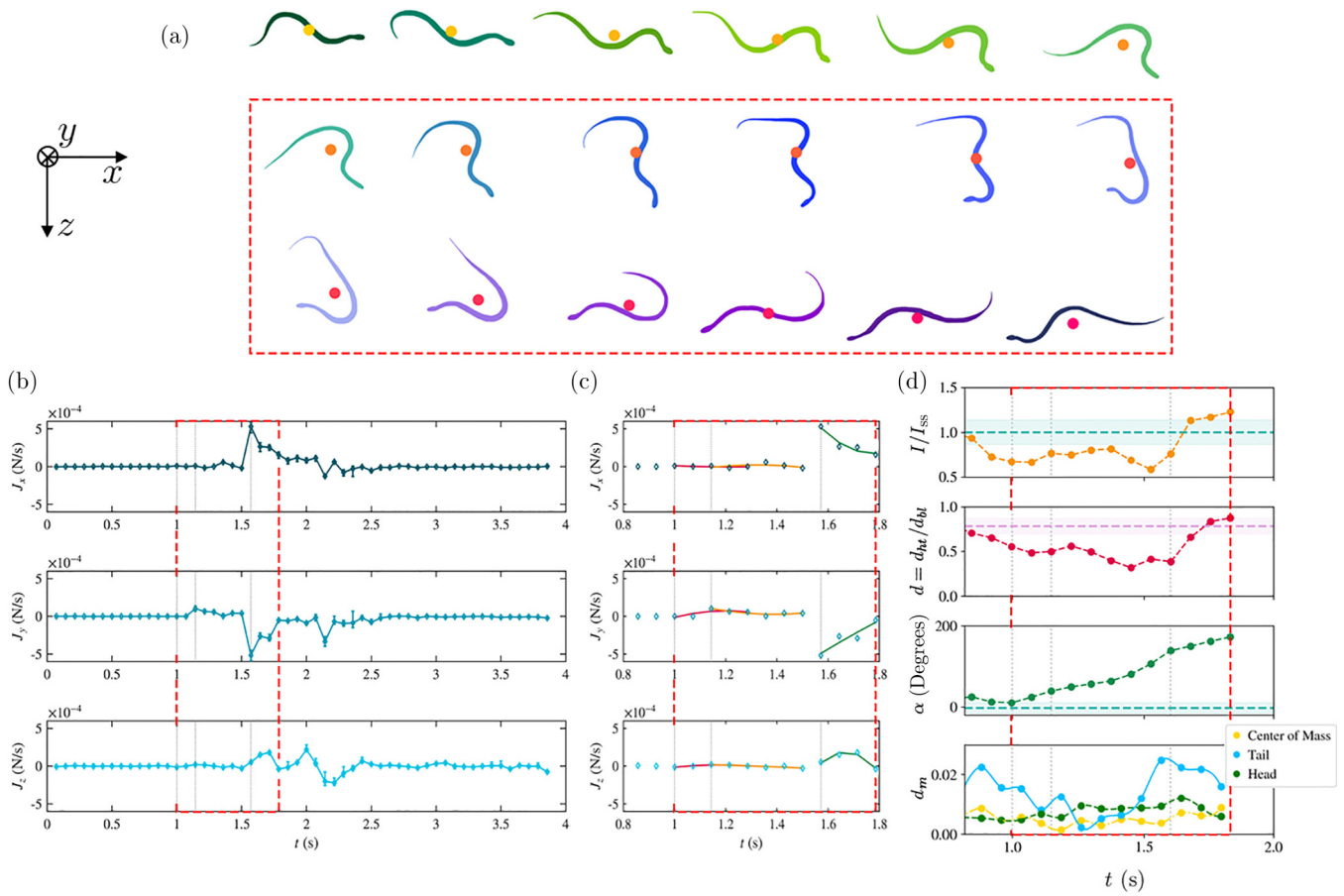

FIG. 6. Results for turn no. 1 (*Natrix maura*): (a) turning kinematics in the x-z plane. (b) Hydrodynamic impulse, $J = [J_x, J_y, J_z]$, error bars indicate sensitivity to $Q \pm 1$. (c) J with quadratic lines of best fit. (d) Turning kinematics quantification. Gray lines indicate moment of first observation for each vortex event, and the turn portion is highlighted by red boxes.

same vortex with a closer view and axis rotated to demonstrate the shape. In Fig. 7 we refer to the snakes that performed turns no. 2 and 6 as individuals no. 2 and 6. The vortex events from turn no. 1 are taken from the time when they first appear in the observation (see red boxes in Fig. 5). The forward swimming vortex events for the individuals that performed turns no. 2 and 6 are shown at their maximum J. This figure demonstrates that all vortex events have a tubular shape. The first vortex observation is composed of one tubular vortex, its pair is likely outside of our measurement volume or too small to resolve. The other five vortex events clearly have pairs with opposite rotations. The tubular vortex pairs that are the best models of hairpin vortices are the third vortex event produced in turn no. 1 and the vortex produced during the forward swimming sequence by individual no. 2. This demonstrates that turning snakes shed vortices of a similar shape to forward swimming snakes.

We quantitatively compare the vortex shedding events by calculating the vortex force. To capture the curve of the data we apply a quadratic polynomial for the line of best fit to the J data points where the vortices are visible [Fig. 6(c) and Fig. 10 in the Appendix]. We take the time derivative of the polynomials and use the slope as the vortex force components. The magnitude and direction of the vortex force is calculated according to convention (see Sec. II) and presented in Table I. In Table I and in the following discussion we refer to the snakes that performed turns no. 2 and 6 as individuals no. 2 and 6.

The vortex force is a representation of the reaction force generated by the snake as it swims. In each case, the direction of the calculated vortex force is opposite to the movement of the snake at that moment. For example, during turn no. 1 the snake generates the third vortex event by uncurling its tail in the positive z direction, so the vortex force is greatest in the negative z direction. There is vortex force in all three directions because fluid movement is always three-dimensional, and while most of the snake's movement is in the x-z plane, there is some along the y axis. These vortex force components follow the results expected according to Newton's third law, in that they travel in the direction opposite to the snake's motion.

We can directly compare the three vortex shedding events observed during the turning sequence using the vortex force magnitude (F_v). In Table I the F_v of the third vortex shedding event is clearly larger than that of the first two. This may be partially due to the overlap of the first two vortex shedding events. Even so, this difference in F_v corresponds with the observation that the size of the third vortex shedding event at $t = 1.57$ in Fig. 5 appears larger than the first two ($t = 1$ and 1.14).

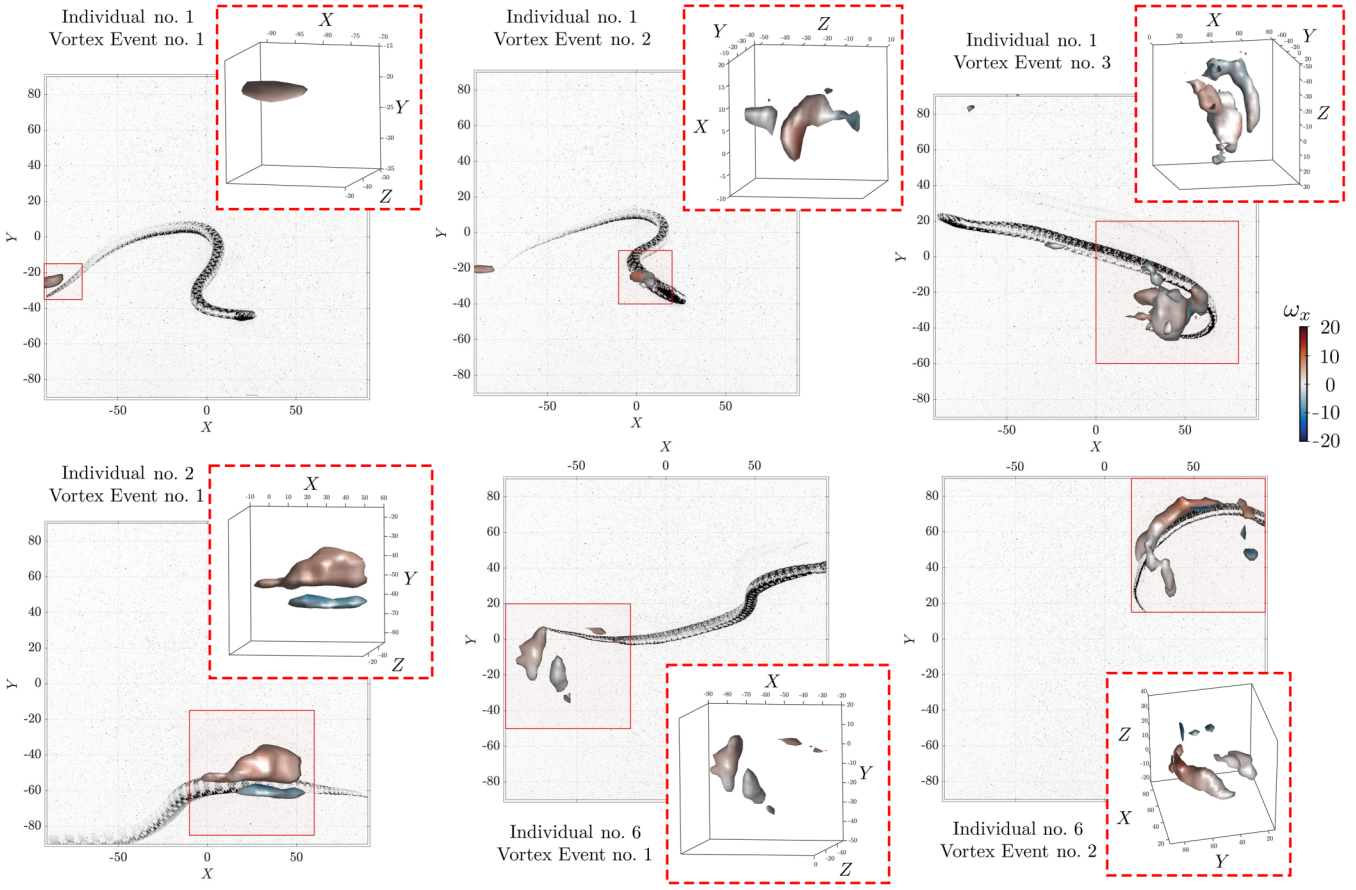

FIG. 7. Vortex event observations for all analyzed vortex events. The red box indicates the region for which we present a closer view of the vortex rotated to show the tubular vortex pairs (individuals who performed turns no. 1 and 6 *Natrix maura*, no. 3 *Nerodia rhombifer*).

The vortex force magnitude (F_v) also allows us to compare between the vortex events generated by the turn and forward swimming sequences. While the snake that performed turn no. 1 is smaller than the one that performed turn no. 2, the largest F_v observed during the turning sequence is 8.6 times larger than the F_v for the forward swimming sequence. The individuals from turning sequences no. 1 and 6 are of more similar sizes, and yet F_v is still 2.5–3 times larger for the third turning vortex event.

Another way we can compare the vortex events between the turn and forward swimming sequences is to calculate the force coefficients. This calculation uses the cross-sectional area of the snake and a characteristic velocity. We will consider two force coefficients: calculated with the velocity for center of mass (com) to consider the overall movement of the snake and then with the velocity of the tail. The results of these calculations can be found in Table I.

The $C_F(U_{\text{com}})$ shows the vortices shed during turn no. 1 are at least 1.23× larger than those shed during the forward swimming sequences. This is especially notable due to the overlap for the first and second turning vortex events, which likely reduces their values for J, F_v and thus, $C_F(U_{\text{com}})$. The third vortex shedding event generated during turn no. 1 is 10.21 times larger than the observation

TABLE I. Quantitative wake results: vortex force ($F_v = \sqrt{F_x + F_y + F_z}$), characteristic velocities (COM, tail, and head where indicated with *), and force coefficients ($CF = Fv/0.5\rho U^2 S$, $S = 0.25D^2\pi$) for individuals who performed turns no. 1 and 6 (*Natrix maura*) and no. 2 (*Nerodia rhombifer*) with $D_{1,2,6} = 0.00769, 0.00893, 0.00652$ m.

Individual	Vortex event	$[F_x, F_y, F_z]$ (N)	F_v (N)	U_{com} (m/s)	U_{tail} (m/s)	$C_F(U_{\text{com}})$	$C_F(U_{\text{tail}})$
1	1	[0.0006, −0.0043, 0.0021]	0.0048	0.057	0.21	63.62	4.69
1	2	[−0.0020, 0.0025, −0.0001]	0.0032	0.052	0.09*	50.96	17.40
1	3	[0.0163, −0.0012, −0.0313]	0.0353	0.086	0.33	205.52	13.96
2	1	[−0.0019, 0.0018, −0.0032]	0.0041	0.081	0.28	20.12	1.68
6	1	[0.0048, 0.0013, −0.0103]	0.0114	0.158	0.46	27.45	3.24
6	2	[−0.0037, −0.0026, 0.0134]	0.0141	0.143	0.38	41.43	5.87

for individual no. 2 and 7.49 and 4.96 times larger than the first and second vortex events observed for individual no. 6, respectively. This significant difference demonstrates that while both gaits rely on vortex shedding, turning requires more intense hydrodynamic events than forward swimming when calculating C_F using the center of mass velocity.

Calculating the force coefficient with the velocity of the tail (or head) changes this comparison. When we look at $C_F(U_{\text{tail}})$ we see that the second vortex produced by the snake's head movement is larger than the third event produced by the tail movement. This is due to the head velocity being significantly smaller than that of the tail. We also see that the $C_F(U_{\text{tail}})$ for the first turning vortex is 0.8× smaller than the second vortex event produced by individual no. 6, as is its F_V and U_{tail}. This is a small difference, and we see a large variation in $C_F(U_{\text{tail}})$ values for the forward swimming vortex events. Still, it is important to note that there are some cases where a turning vortex is not larger than in forward swimming.

IV. CONCLUSION

Our results demonstrate that snakes rearrange their body position and center of mass when turning to reduce their moment of inertia, similarly to zebrafish and jellyfish [17]. We report the change in moment of inertia throughout six unique turns completed by six snakes. In most examples they oscillate between relatively high and low moments of inertia, where the high values are within the range for forward swimming and the lower values are outside. The snakes decrease their moment of inertia by drawing their head and tail closer together more drastically when turning over a shorter time frame and a smaller turning radius. The variety of observed turning behaviors demonstrates the diversity of ways anguilliform swimmers can change swimming direction.

Snakes use their entire body surface to accelerate fluid and propel themselves when swimming. We report volumetric wake measurements taken during the voluntary turn no. 1 to show how the vortex shedding is related to the kinematics. Our results indicate that the snake rearranges its body to change the moment of inertia before shedding a vortex to turn. We quantify the vortex shedding events by calculating the hydrodynamic impulse and taking the time derivative to find the vortex force. The vortex observation with the largest vortex force is produced when the snake exits turn no. 1 and is 2.5–8.6× larger than those observed during forward swimming. We calculate force coefficients using the characteristic velocities for center of mass (com) and tail to directly compare turn no. 1's with the forward swimming sequences. The $C_F(U_{\text{com}})$ revealed that the vortices shed during turn no. 1 are between 1.23 and 10.21 times larger than the vortices shed during forward swimming sequences. The $C_F(U_{\text{tail}})$ revealed that the vortex shed as the snake entered turn no. 1 was within the range of observations for the forward swimming vortices. Our observations show that snakes shed vortices of various sizes when turning, including some that are significantly larger. Similar to the larger vortices created by fish performing the C-start [14]. Finally, our volumetric wake measurements show that all observations have the same tubular vortex pair composition as those in Stin *et al.* [4].

These results highlight the link between anguilliform swimmers' turning maneuvers and those employed by swimmers with entirely different propulsion systems. While they have a different mode of swimming, they still reduce their moment of inertia and generate larger vortices when turning. These experimental observations can inform future computational investigations into anguilliform turning to fully compute the forces. This interpretation of turning will be broadly applicable for elongated swimmers and bio-inspired robots.

ACKNOWLEDGMENTS

We would like to thank the interns that aided E.G. with data collection: Olivia Alves, Lauréanne Feral, and Johannes Marchand. This work is funded by the Agence Nationale de la Recherche (France) through project DRAGON2 (ANR-20-CE02-0010). The snake handling protocol complies with the European Directive 2010/63/EU for the protection of animals used for scientific purposes.

DATA AVAILABILITY

The data that support the findings of this article are publicly available [31] and the code used to analyze the data is available at [32,33].

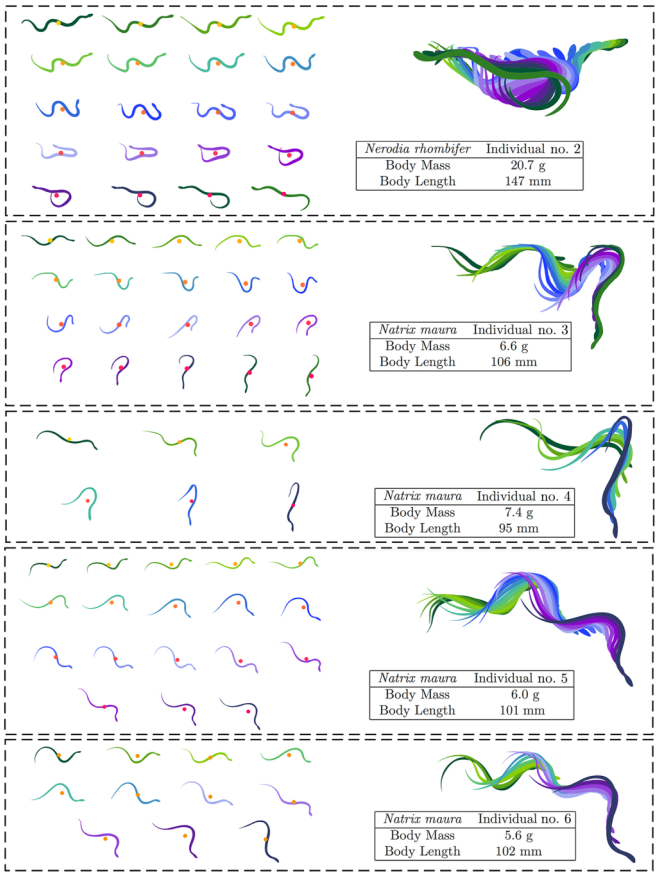

FIG. 8. Kinematics of observed turns for individuals no. 2–6: (left) center of mass location while turning, (right) superimposed kinematics and body size measurements.

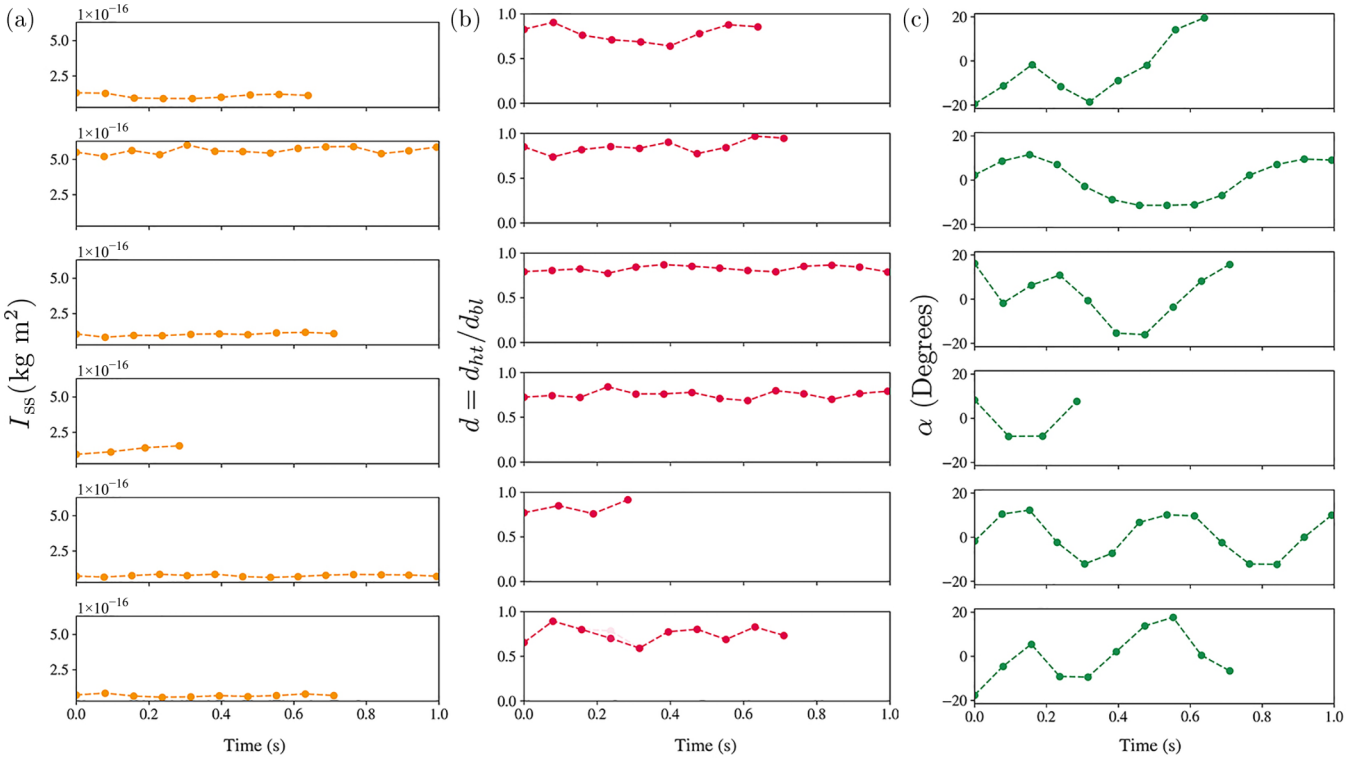

FIG. 9. Quantitative results for forward swimming sequences for individuals no. 1–6: (a) moment of inertia (kg m^2), (b) distance between head and tail (d), and (c) angle between head and tail (α) (individuals no. 1 and 3–6 *Natrix maura*, individual no. 2 *Nerodia rhombifer*).

APPENDIX

In this study, we consider six turning sequences by six snakes. The full results for turn no. 1 are included in the body of this paper, and this appendix includes the results for the other five turning sequences. Figure 8 shows the kinematics of each of the turning sequences with the center of mass for the snake at each moment in time as well as their superimposed kinematics and measurements. In Fig. 8 and throughout this appendix we refer to the snakes that performed turns no. 2–6 as individuals no. 2–6.

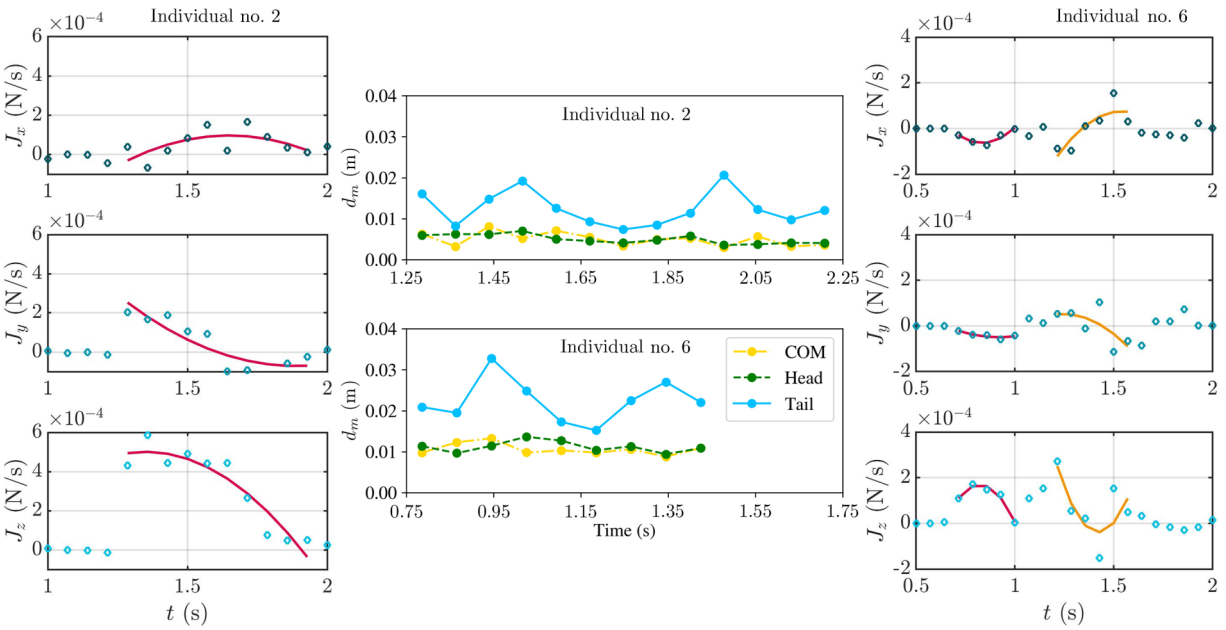

FIG. 10. Displacement during forward swimming and hydrodynamic impulse measurements with quadratic best fit lines for individuals no. 2 and 6 (*Nerodia rhombifer* and *Natrix maura,* respectively).

We quantify the swimming kinematics by calculating the estimated moment of inertia, as well as the distance and the angle between the snake's head and tail [see Eqs. (3)–(5)]. The results for the forward swimming sequences of all six individuals are shown in Fig. 9. It demonstrates the small range of values forward swimming snakes have for I_{SS} and d. Individual no. 2 has a higher moment of inertia relative to the other five individuals due to its greater mass (see Fig. 8). The α typically oscillates between high and low values; individual no. 3 exhibits the largest amplitude reaching nearly 30°. We also quantify forward swimming by calculating the hydrodynamic impulse for individuals no. 2 and 6 vortex observations. The maximum J for each of these vortex events in Fig. 10 demonstrate the smaller size of these vortices compared to the turning results (Fig. 6).

[1] V. Stin, R. Godoy-Diana, X. Bonnet, and A. Herrel, Form and function of anguilliform swimming, Biol. Rev. **99**, 2190 (2024).

[2] U. K. Müller, J. Smit, E. J. Stamhuis, and J. J. Videler, How the body contributes to the wake in undulatory fish swimming: Flow fields of a swimming eel (*Anguilla anguilla*), J. Exp. Biol. **204**, 2751 (2001).

[3] B. J. Gemmell, S. M. Fogerson, J. H. Costello, J. R. Morgan, J. O. Dabiri, and S. P. Colin, How the bending kinematics of swimming lampreys build negative pressure fields for suction thrust, J. Exp. Biol. **219**, 3884 (2016).

[4] V. Stin, R. Godoy-Diana, X. Bonnet, and A. Herrel, Measuring the 3D wake of swimming snakes (*Natrix tessellata*) using volumetric particle image velocimetry, J. Exp. Biol. **226**, jeb245929 (2023).

[5] S. Kern and P. Koumoutsakos, Simulations of optimized anguilliform swimming, J. Exp. Biol. **209**, 4841 (2006).

[6] I. Borazjani and F. Sotiropoulos, Numerical investigation of the hydrodynamics of anguilliform swimming in the transitional and inertial flow regimes, J. Exp. Biol. **212**, 576 (2009).

[7] P. W. Webb, Form and function in fish swimming, Sci. Am. **251**, 72 (1984).

[8] A. Herrel, H. F. Choi, E. Dumont, N. De Schepper, B. Vanhooydonck, P. Aerts, and D. Adriaens, Burrowing and subsurface locomotion in anguilliform fish: Behavioral specializations and mechanical constraints, J. Exp. Biol. **214**, 1379 (2011).

[9] J. Herault, É. Clement, J. Brossillon, S. LaGrange, V. Lebastard, and F. Boyer, Standing on the water: Stability mechanisms of snakes on free surface, in *Biomimetic and Biohybrid Systems: 9th International Conference, Living Machines 2020, Freiburg, Germany, July 28–30, 2020, Proceedings 9* (Springer, Berlin, 2020), pp. 165–175.

[10] K. D'Août and P. Aerts, A kinematic comparison of forward and backward swimming in the eel *Anguilla anguilla*, J. Exp. Biol. **202**, 1511 (1999).

[11] B. C. Jayne, What defines different modes of snake locomotion? Integr. Comp. Biol. **60**, 156 (2020).

[12] P. Domenici and R. W. Blake, The kinematics and performance of fish fast-start swimming, J. Exp. Biol. **200**, 1165 (1997).

[13] M. Gazzola, W. M. Van Rees, and P. Koumoutsakos, C-start: Optimal start of larval fish, J. Fluid Mech. **698**, 5 (2012).

[14] M. S. Triantafyllou, G. S. Triantafyllou, and D. K. P. Yue, Hydrodynamics of fishlike swimming, Annu. Rev. Fluid Mech. **32**, 33 (2000).

[15] G. Li, U. K. Müller, J. L. van Leeuwen, and H. Liu, Escape trajectories are deflected when fish larvae intercept their own C-start wake, J. R. Soc. Interface **11**, 20140848 (2014).

[16] A. Clark and E. Tytell, Fast turns are not sped up slow turns: How bluegill sunfish change their kinematics with turn speed, bioRxiv (2025).

[17] J. O. Dabiri, S. P. Colin, B. J. Gemmell, K. N. Lucas, M. C. Leftwich, and J. H. Costello, Jellyfish and fish solve the challenges of turning dynamics similarly to achieve high maneuverability, Fluids **5**, 106 (2020).

[18] J. H. Costello, S. P. Colin, B. J. Gemmell, J. O. Dabiri, and E. A. Kanso, Turning kinematics of the scyphomedusa *Aurelia aurita*, Bioinspir. Biomim. **19**, 026005 (2024).

[19] I. K. Bartol, A. M. Ganley, A. N. Tumminelli, P. S. Krueger, and J. T. Thompson, Vectored jets power arms-first and tail-first turns differently in brief squid with assistance from fins and keeled arms, J. Exp. Biol. **225**, jeb244151 (2022).

[20] R. Thandiackal and G. V. Lauder, How zebrafish turn: Analysis of pressure force dynamics and mechanical work, J. Exp. Biol. **223**, jeb.223230 (2020).

[21] D. J. Li and L. Mendelson, Volumetric measurements of wake impulse and kinetic energy for evaluating swimming performance, Exp. Fluids **64**, 47 (2023).

[22] C. Ye, S. Ma, B. Li, and Y. Wang, Turning and side motion of snake-like robot, in *IEEE International Conference on Robotics and Automation, 2004. Proceedings. ICRA'04. 2004* (IEEE, New York, 2004), Vol. 5, pp. 5075–5080.

[23] H. Shi, W. Cui, Y. Meng, S. Wang, and Y. Xie, Steering through waters: Exploring turning control techniques for soft underwater snake robots, in *2023 IEEE International Conference on Robotics and Biomimetics (ROBIO)* (IEEE, New York, 2023), pp. 1–7.

[24] T. Wang, B. Chong, K. Diaz, J. Whitman, H. Lu, M. Travers, D. I. Goldman, and H. Choset, The omega turn: A biologically-inspired turning strategy for elongated limbless robots, in *2020 IEEE/RSJ International Conference on Intelligent Robots and Systems (IROS)* (IEEE, New York, 2020), pp. 7766–7771.

[25] T. Wang, B. Chong, Y. Deng, R. Fu, H. Choset, and D. I. Goldman, Generalized omega turn gait enables agile limbless robot turning in complex environments, in *2022 International Conference on Robotics and Automation (ICRA)* (IEEE, New York, 2022), pp. 01–07.

[26] A. Anastasiadis, A. Rossi, L. Paez, K. Melo, E. D. Tytell, A. J. Ijspeert, and K. Mulleners, Eel-like robot swims more efficiently with increasing joint amplitudes compared to constant joint amplitudes, Phys. Rev. Fluids **9**, 110509 (2024).

[27] F. Pereira and M. Gharib, Defocusing digital particle image velocimetry and the three-dimensional characterization of two-phase flows, Meas. Sci. Technol. **13**, 683 (2002).

[28] P. G. Saffman, *Vortex Dynamics* (Cambridge University Press, Cambridge, 1992).

[29] C. Gong, M. J. Travers, H. C. Astley, L. Li, J. R. Mendelson, D. I. Goldman, and H. Choset, Kinematic gait synthesis for snake robots, Int. J. Robot. Res. **35**, 100 (2016).

[30] P. Virtanen, R. Gommers, T. E. Oliphant, M. Haberland, T. Reddy, D. Cournapeau, E. Burovski, P. Peterson, W. Weckesser, J. Bright, S. J. van der Walt, M. Brett, J. Wilson, K. J. Millman, N. Mayorov, A. R. J. Nelson, E. Jones, R. Kern, E. Larson, C. J. Carey, *et al.*, SciPy 1.0: Fundamental algorithms for scientific computing in Python, Nat. Methods **17**, 261 (2020).

[31] E. Gregorio, R. Godoy-Diana, and A. Herrel, Swimming kinematics and volumetric wake measurements for *Natrix maura* and *Nerodia rhombifer*, data. InDoRES platform (2026), https://doi.org/10.48579/PRO/5Q27ST.

[32] E. Gregorio, V. Stin, R. Godoy-Diana, and A. Herrel, egregorio/Snake-Swimming-Vortex-Code: Turning without fins 3D PIV code (Version v1.0.0) [Computer software], Zenodo, 2026, https://doi.org/10.5281/zenodo.21564012.

[33] E. Gregorio, R. Godoy-Diana, and A. Herrel, egregorio/Snake-Swimming-Kinematics Turning without fins swimming kinematics code (Version v1.0.0) [Computer software], Zenodo, 2026, https://doi.org/10.5281/zenodo.21564055.